

Ionothermal Synthesis, Crystal Structure, and Magnetic Study of $\text{Co}_2\text{PO}_4\text{OH}$ Isostructural with Caminite

Guangmei Wang,[†] Martin Valldor,[⊥] Eike T. Spielberg,[†] and Anja-Verena Mudring*,^{†,‡,§}

[†]Inorganic Chemistry III—Materials Engineering and Characterization, Ruhr-Universität Bochum, D-44780 Bochum, Germany

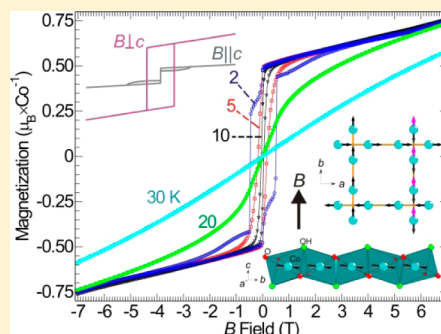
[‡]Materials Science and Engineering, Iowa State University, Ames, Iowa 50011, United States

[§]Critical Materials Institute, Ames Laboratory, Ames, Iowa 50011, United States

[⊥]Physics of Correlated Matter, Max-Planck-Institute for Chemical Physics of Solids, D-01187 Dresden, Germany

Supporting Information

ABSTRACT: A new framework cobalt(II) hydroxyl phosphate, $\text{Co}_2\text{PO}_4\text{OH}$, was prepared by ionothermal synthesis using 1-butyl-4-methyl-pyridinium hexafluorophosphate as the ionic liquid. As the formation of $\text{Co}_2\text{PO}_4\text{F}$ competes in the synthesis, the synthesis conditions have to be judiciously chosen to obtain well-crystallized, single phase $\text{Co}_2\text{PO}_4\text{OH}$. Single-crystal X-ray diffraction analyses reveal $\text{Co}_2\text{PO}_4\text{OH}$ crystallizes with space group $I4_1/\text{amd}$ ($a = b = 5.2713(7)$ Å, $c = 12.907(3)$ Å, $V = 358.63(10)$ Å³, and $Z = 4$). Astonishingly, it does not crystallize isotropically with $\text{Co}_2\text{PO}_4\text{F}$ but rather isotropically with the hydroxyl minerals caminite $\text{Mg}_{1.33}[\text{SO}_4(\text{OH})_{0.66}(\text{H}_2\text{O})_{0.33}]$ and lipscombeite $\text{Fe}_{2-y}\text{PO}_4(\text{OH})$ ($0 \leq y \leq 2/3$). Phosphate tetrahedra groups interconnect four rod-packed face-sharing $\{\text{CoO}_{6/2}\}$ octahedra chains to form a three-dimensional framework structure. The compound $\text{Co}_2\text{PO}_4\text{OH}$ was further characterized by powder X-ray diffraction, Fourier transform–infrared, and ultraviolet–visible spectroscopy, confirming the discussed structure. The magnetic measurement reveals that $\text{Co}_2\text{PO}_4\text{OH}$ undergoes a magnetic transition and presents at low temperatures a canted antiferromagnetic spin order in the ground state.



INTRODUCTION

Phosphorus is the 10th most abundant element on earth and tends to be concentrated in igneous rocks.¹ Naturally occurring phosphate minerals have rich crystal chemistry; the major constituents of phosphorite are the minerals of the apatite group.² A large number of structurally and chemically diverse synthetic metallophosphates³ are extensively studied with respect to a wide range of applications, such as ion exchange,⁴ catalysis,⁵ adsorption,⁶ nonlinear optics,⁷ and battery materials.⁸

Since cobalt phosphate was used as a component in semiconductive glasses,⁹ such materials have attracted renewed interest in the field of ion-selective microelectrodes, catalysts, battery electrodes, and glass materials.¹⁰ Furthermore, cobalt phosphate has been studied as a solid-state catalyst in the solar light-induced oxidation of water to O₂.^{10b} Current cobalt phosphates are being extensively studied as cathode materials for rechargeable lithium ion batteries to increase energy storage and voltage output.^{10c}

In the field of open-framework metallophosphates, cobalt phosphates are of particular interest as Co²⁺ is one of the few transition-metal cations that not only can adopt an octahedral but also a tetrahedral coordination environment and thus is able to substitute silicon or phosphorus in silicates and phosphates. The incorporation of cobalt cations into zeolites can improve the catalytic performance of the material.¹¹ In addition, cobalt phosphates are of interest because of their

magnetic properties.¹² Since the first amino-templated tetrahedral open framework cobalt phosphate [C₂H₁₀N₂]₂[CoPO₄] was reported in 1994, much attention has been paid to this class of compounds.¹³

Recently, our group successfully utilized ionic liquids (ILs) in the synthesis of metal, metal fluoride, and metal oxide nanomaterials for energy-related applications, for example, in catalysis or photonic materials.¹⁴ At the same time, we have explored a wide range of ILs with different cations and anions in the synthesis of layered and framework alumophosphates,¹⁵ a new aluminum fluoride hexahydrate, a new open-framework iron borophosphate,¹⁶ and a manganese borophosphate, KMnBP₂O₇(OH)₂.¹⁷ The advantage of tetrafluoroborate or hexafluorophosphate ionic liquids in the synthesis of metal phosphates is that such ionic liquids can not only serve as the solvent and template but also as the mineralizer, because of the release of fluoride anions during the reaction.

We describe herein how this process can be used to prepare, by a judicious choice of the reaction parameters, highly crystalline single-phased $\text{Co}_2\text{PO}_4\text{OH}$, whose magnetic susceptibility will be described.

Received: December 4, 2013

Published: March 5, 2014



Table 1. Details of Initial Mixture and Crystallization Conditions for the Preparation of $\text{Co}_2\text{PO}_4\text{OH}$

sample	composition	T (°C)	t (d)	product
S1	variation of the IL amount $\text{Co}(\text{OAc})_2 \cdot 4\text{H}_2\text{O} : \text{H}_3\text{PO}_4 : 0.75\text{H}_3\text{BO}_3 : [\text{C}_4\text{mpy}] [\text{PF}_6]$	200	7	(1)
S2	$\text{Co}(\text{OAc})_2 \cdot 4\text{H}_2\text{O} : \text{H}_3\text{PO}_4 : 0.75\text{H}_3\text{BO}_3 : 0.5[\text{C}_4\text{mpy}] [\text{PF}_6]$	200	7	(1) + (2)
S3	$\text{Co}(\text{OAc})_2 \cdot 4\text{H}_2\text{O} : \text{H}_3\text{PO}_4 : 0.75\text{H}_3\text{BO}_3 : 0.25[\text{C}_4\text{mpy}] [\text{PF}_6]$	200	7	unknown phase
S4	$\text{Co}(\text{OAc})_2 \cdot 4\text{H}_2\text{O} : \text{H}_3\text{PO}_4 : 0.75\text{H}_3\text{BO}_3 : 2[\text{C}_4\text{mpy}] [\text{PF}_6]$ different amount of $\text{Co}(\text{OAc})_2$	200	7	(1) + amorphous
S5	$1.2\text{Co}(\text{OAc})_2 \cdot 4\text{H}_2\text{O} : \text{H}_3\text{PO}_4 : 0.75\text{H}_3\text{BO}_3 : [\text{C}_4\text{mpy}] [\text{PF}_6]$	200	7	(1) \gg (2)
S6	$1.8\text{Co}(\text{OAc})_2 \cdot 4\text{H}_2\text{O} : \text{H}_3\text{PO}_4 : 0.75\text{H}_3\text{BO}_3 : [\text{C}_4\text{mpy}] [\text{PF}_6]$ different amount of H_3PO_4	200	7	(2) \gg (1)
S7	$\text{Co}(\text{OAc})_2 \cdot 4\text{H}_2\text{O} : 2\text{H}_3\text{PO}_4 : \text{H}_3\text{BO}_3 : [\text{C}_4\text{mpy}] [\text{PF}_6]$	200	7	(1)
S8	$\text{Co}(\text{OAc})_2 \cdot 4\text{H}_2\text{O} : (2/3)\text{H}_3\text{PO}_4 : \text{H}_3\text{BO}_3 : [\text{C}_4\text{mpy}] [\text{PF}_6]$ different amount of H_3BO_3	200	7	(1) + (2)
S9	$\text{Co}(\text{OAc})_2 \cdot 4\text{H}_2\text{O} : \text{H}_3\text{PO}_4 : 0 - 0.75\text{H}_3\text{BO}_3 : [\text{C}_4\text{mpy}] [\text{PF}_6]$	200	7	(1)
S10	$\text{Co}(\text{OAc})_2 \cdot 4\text{H}_2\text{O} : \text{H}_3\text{PO}_4 : 1\text{H}_3\text{BO}_3 : [\text{C}_4\text{mpy}] [\text{PF}_6]$	200	7	(2)

EXPERIMENTAL SECTION

Syntheses. $\text{Co}_2\text{PO}_4\text{OH}$ is prepared under ionothermal conditions using the IL 1-butyl-4-methylpyridinium hexafluorophosphate $[\text{C}_4\text{mpy}] [\text{PF}_6]$ as the solvent. In a typical reaction, a mixture of cobalt(II) acetate tetrahydrate ($\text{Co}(\text{OAc})_2 \cdot 4\text{H}_2\text{O}$, 98%, ACROS), phosphoric acid (H_3PO_4 , 85%, J. T. Baker), and $[\text{C}_4\text{mpy}] [\text{PF}_6]$ (99%, Merck) is reacted in a 3 mL Teflon-lined stainless steel autoclave at 200 °C for 7 d, followed by cooling to room temperature. The products were filtered off by suction, washed with deionized water and acetone, and dried at 60 °C for 1 d. Phase purity of the product was confirmed by the agreement between the experimental powder X-ray diffraction (PXRD) patterns and the simulated patterns based on the single-crystal structure analysis (Supporting Information, Figure S1).

Single-Crystal Structure Determination. A suitable single crystal of $\text{Co}_2\text{PO}_4\text{OH}$ with dimensions of $0.12 \times 0.02 \times 0.02$ mm was selected for single-crystal X-ray diffraction (SXRD) analysis. The data were collected at ambient temperature using graphite-monochromated Mo K α radiation on an Image Plate Diffraction System, IPDS I (Stoe, Darmstadt, Germany). The data were corrected for Lorentz and polarization effects. Data correction was carried out with the program X-RED.¹⁸ A face-indexed numerical absorption correction (X-SHAPE) was applied.¹⁹ The structure was solved by direct methods and refined by full-matrix least-squares techniques with the SHELXTL crystallographic software package.²⁰ The Co, P, and O atoms could be unambiguously located. See Supporting Information for experimental details on the crystal structure determination of $\text{Co}_2\text{PO}_4\text{OH}$ and for further details of the crystal structure investigations.

Characterizations. PXRD data were collected on an image plate-G670 Guinier camera (Huber, Rimsting, Germany) with Mo K α radiation $\lambda = 0.71073$ Å. FT-IR spectra were measured on a Bruker Alpha spectrometer with KBr pellets in the range of 4000–400 cm⁻¹. Ultraviolet-visible (UV-vis) absorption spectra were measured on an Agilent Cary 5000 spectrometer on a solid sample, using the internal diffuse reflection accessory. To avoid saturation, samples were ground with a 10-fold excess of BaSO_4 prior to the measurements. The reflectance spectrum recorded of pure optical-grade BaSO_4 was used as reference.

Magnetism. The magnetic susceptibility of $\text{Co}_2\text{PO}_4\text{OH}$ was measured in a MPMS-XL7 apparatus (Quantum Design) on powder samples placed in a polycarbonate capsule and fixed with high purity inert wax to prevent the powder from moving under the influence of the applied high magnetic fields. Both the direct current (dc) and alternating current (ac) magnetic susceptibilities (χ) were measured. For determination of the dc magnetic susceptibility, a field of 0.1 T was used for the temperature-dependent measurement, and fields up to 7 T were used for the isothermal magnetizations at temperatures of 2, 5, 10, 20, and 30 K. The driving field in the ac measurements was 2 Oe, with frequencies ranging from 1 to 1000 Hz.

RESULTS AND DISCUSSION

Synthesis and Characterization. The original objective of our experiments was to produce complex cobalt hydroxyphosphates. Surprisingly, we obtained two different compounds, $\text{Co}_2\text{PO}_4\text{OH}$ (1) and $\text{Co}_2\text{PO}_4\text{F}$ (2), under quite similar synthesis conditions, using the IL 1-butyl-4-methylpyridinium hexafluorophosphate $[\text{C}_4\text{mpy}] [\text{PF}_6]$ as the solvent and mineralizer. It was found that $\text{Co}_2\text{PO}_4\text{OH}$ (1) crystallizes in the space group $I4_1/\text{amd}$, isotopic with the minerals caminite ($\text{Mg}_{1.33}[\text{SO}_4(\text{OH})_{0.66}(\text{H}_2\text{O})_{0.33}]$) and lipscombite $\text{Fe}_{2-y}\text{PO}_4(\text{OH})$ ($0 \leq y \leq 2/3$).²¹ The competing phase, $\text{Co}_2\text{PO}_4\text{F}$ (2),²² crystallizes isostructurally with triplite ($\text{Mn}_2\text{PO}_4\text{F}$)²³ with the space group $C2/c$. To elucidate the mechanism of formation of $\text{Co}_2\text{PO}_4\text{X}$ ($\text{X} = \text{OH}, \text{F}$), a systematic synthesis study was carried out. We explored the variation of various parameters such as stoichiometric ratios and concentrations of the starting materials. Table 1 summarizes the initial mixture compositions, crystallization conditions, and the phases obtained. By a careful choice of the reaction parameters we managed to obtain monophasic $\text{Co}_2\text{PO}_4\text{OH}$ (1).

Pure $\text{Co}_2\text{PO}_4\text{OH}$ (1) could be obtained by heating a molar composition of $\text{Co}(\text{OAc})_2 \cdot 4\text{H}_2\text{O}$ (OAc = acetate), H_3PO_4 , and 0.75 H_3BO_3 in $[\text{C}_4\text{mpy}] [\text{PF}_6]$ in a ratio of 1:1:0.75:1 at 200 °C for 7 d (sample S1). Upon halving the amount of the IL $[\text{C}_4\text{mpy}] [\text{PF}_6]$, a mixture of $\text{Co}_2\text{PO}_4\text{OH}$ (1) and $\text{Co}_2\text{PO}_4\text{F}$ (2) was obtained (sample S2). When further decreasing the amount of the IL, a new, unknown phase of poor crystallinity formed, and $\text{Co}_2\text{PO}_4\text{OH}$ (1) could no longer be observed (sample S3). When doubling the amount of $[\text{C}_4\text{mpy}] [\text{PF}_6]$, $\text{Co}_2\text{PO}_4\text{OH}$ (1) was obtained along with an amorphous pink powder (sample S4). When the amount of $\text{Co}(\text{OAc})_2 \cdot 4\text{H}_2\text{O}$ was increased, biphasic mixtures of $\text{Co}_2\text{PO}_4\text{OH}$ (1) and $\text{Co}_2\text{PO}_4\text{F}$ (2) formed (sample S5), with (1) being dominant for increases of up to 1.5 times the original amount and (2) becoming the prevalent species thereafter (sample S6). Increases of up to double the amount of H_3PO_4 still led to pure $\text{Co}_2\text{PO}_4\text{OH}$ (1) (sample S7), whereas decreases gave both $\text{Co}_2\text{PO}_4\text{OH}$ (1) and $\text{Co}_2\text{PO}_4\text{F}$ (2) in biphasic samples (sample S8). The initial pH of the starting mixtures was adjusted by H_3BO_3 . $\text{Co}_2\text{PO}_4\text{OH}$ (1) with good purity could be obtained with amounts of H_3BO_3 between 0 and 0.75 mmol (sample S9). However, when H_3BO_3 levels were increased from 0.75 to 1 mmol, pure $\text{Co}_2\text{PO}_4\text{F}$ (2) was obtained (sample S10).

The thermal stability of $\text{Co}_2\text{PO}_4\text{OH}$ in air was determined using thermal gravimetric analysis, and the results are shown in

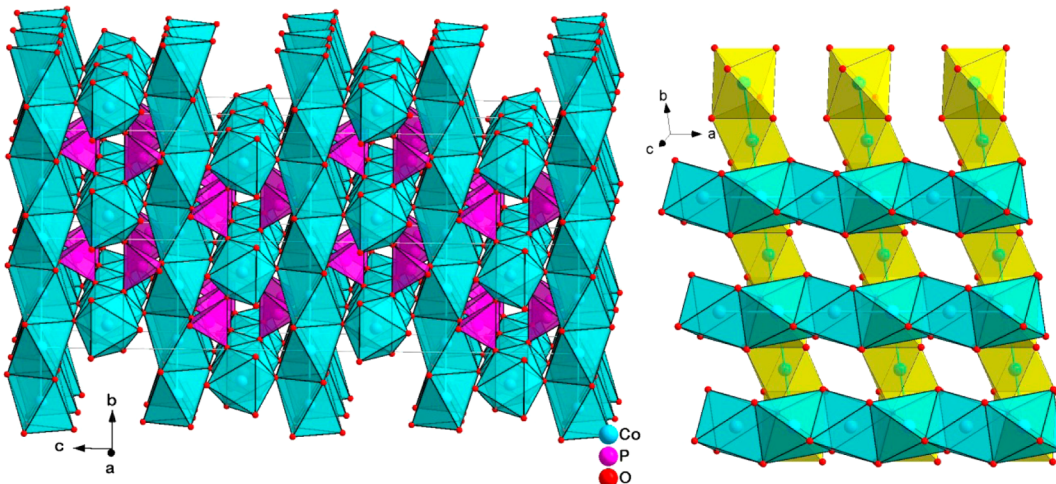


Figure 1. (left) Perspective view of the 3D framework structure of $\text{Co}_2\text{PO}_4\text{OH}$ (1) along the [100] direction. (right) A view along the [111] direction showing the rod-packing of face-sharing $\frac{1}{2}\{\text{CoO}_{6/2}\}$ octahedral chains parallel to [100] (blue) and [010] (yellow).

Supporting Information, Figure S2. $\text{Co}_2\text{PO}_4\text{OH}$ remains stable under ambient conditions up to 400 °C, while $\text{Co}_2\text{PO}_4\text{F}$ is stable up to 1000 °C.

Crystal Structure. Single-crystal structure analysis reveals that $\text{Co}_2\text{PO}_4\text{OH}$ crystallizes in the tetragonal unit cell with space group $I4_1/\text{amd}$ (No. 141). The cell parameters are $a = b = 5.2713(7)$ Å, $c = 12.907(3)$ Å, $V = 358.63(10)$ Å³, and $Z = 4$. For further structural details such as an atomic coordinate list and selected bond lengths and angles see Supporting Information. The structure of $\text{Co}_2\text{PO}_4\text{OH}$ is characterized by a three-dimensional (3D) framework of $\{\text{CoO}_4(\text{OH})_2\}$ octahedra and monophosphate $[\text{PO}_4]$ tetrahedra. The asymmetric unit of the crystal structure contains four crystallographically distinct atoms, one cobalt atom, one phosphorus atom, one oxygen atom, and one hydroxyl ion (Supporting Information, Figure S3). The cobalt atom is located on an inversion center (Wyckoff position 8 c) and has an octahedral coordination to four oxygen atoms located on a mirror plane (Wyckoff position 16 h) and two hydroxyl ions located on the cross point of an inversion axis $\bar{4}$, a mirror plane, and a 2-fold axis (Wyckoff position 4 a). The $\text{Co}(1)-\text{O}(1)$ and $\text{Co}(1)-\text{O}(1\text{H})$ bond lengths are 2.064(6) Å and 2.0832(3) Å, respectively. The cis $\text{O}-\text{Co}-\text{O}$ bond angles range from 82.6(2)° to 97.4(2)°, whereas the trans angles are 180°. The phosphorus atom is located on the cross point of an inversion axis $\bar{4}$, a mirror plane, and a 2-fold axis (Wyckoff position 4 b), and is involved in eight $\text{P}-\text{O}-\text{Co}$ bonds via four bridging oxygen atoms. The phosphate tetrahedra are quite regular, with $\text{P}-\text{O}$ bond distances of 1.510(8) Å and with $\text{O}-\text{P}-\text{O}$ angles varying from 108.7(7) to 109.9(4)°. All the oxygen atoms in the structure are three-coordinated bridging atoms, which lead to $\text{Co}-\text{O}-\text{Co}$, $\text{Co}-\text{O}(\text{H})-\text{Co}$, and $\text{P}-\text{O}-\text{Co}$ linkages.

$\text{Co}_2\text{PO}_4\text{OH}$ consists of chains of face-sharing $\frac{1}{2}\{\text{CoO}_{6/2}\}$ octahedra along [100] and [010] connected by phosphate groups as shown in Figure 1. The $\text{CoO}_4(\text{OH})_2$ octahedra are connected to each other through two $\text{O}(1)$ and one $\text{O}(1\text{H})$ atoms forming face-sharing chains along the a and b axes (Figure 1, right). These face-sharing cobalt octahedra chains are linked together via bridging $\text{O}(1\text{H})$ atoms forming a simple 3D rod-packing structure, following the concept of O’Keeffe and Andersson,²⁴ with six-membered rings along the a and b axes. Phosphate tetrahedral groups interconnect four of these $\text{CoO}_4(\text{OH})_2$ octahedra chains to generate a 3D framework.

FT-IR Spectroscopy. An FT-IR spectrum for $\text{Co}_2\text{PO}_4\text{OH}$ recorded in the region of 4000–400 cm⁻¹ was collected to confirm the presence of $\text{Co}-\text{O}-\text{H}$ moieties (Figure 2). The

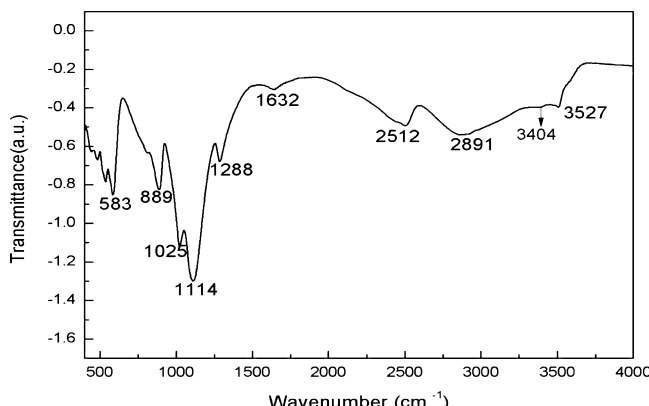


Figure 2. FT-IR spectrum of $\text{Co}_2\text{PO}_4\text{OH}$ (1) measured with KBr pellets in the range of 4000–400 cm⁻¹. The spectrum shows bands caused by $\text{Co}-\text{O}-\text{H}$ moieties and PO_4 groups discussed in the text.

peak observed at 3527 cm⁻¹ can be attributed to the stretching vibration of the bridging –OH group of the octahedral $\text{CoO}_4(\text{OH})_2$. Moreover, it is possible to observe another weak and broad band at around 3404 cm⁻¹, which is assigned to stretching vibrations of $\text{Co}-\text{O}-\text{H}$ groups as was shown in $[\text{Co}_{1.7}\text{Mn}_{0.3}(\text{OH})\text{PO}_4]$ and $\text{Co}_2(\text{OH})(\text{PO}_4)_{1-x}(\text{AsO}_4)_x$ ($0 \leq x \leq 1$).²⁵ The two broad absorption bands in the neighborhood of 2891 and 2512 cm⁻¹ are frequently interpreted as a doublet produced by the $\text{O}(1\text{H})-\text{H}\cdots\text{O}(1)$ stretching vibration split by proton tunneling between two equilibrium positions along the $\text{O}-\text{O}$ axis ($d_{\text{O}(1\text{H})\cdots\text{O}(1)} = 2.7379(89)$ Å).²⁶

The peak at 889 cm⁻¹ is assigned to the bridging –OH in the $\text{Co}-\text{OH}-\text{Co}$ bending vibration²⁷ as was shown in $\text{NaCo}_3(\text{OH})(\text{PO}_4)_2 \cdot (1/4)\text{H}_2\text{O}$.²⁸ These large absorption bands together with the weak peak at 1632 cm⁻¹ indicate the presence of OH groups in the $\text{Co}_2\text{PO}_4\text{OH}$ (1) structure.^{25a} The bands at around 1114 cm⁻¹ and 1025 cm⁻¹ are attributed to the asymmetric stretching vibration of the phosphate tetrahedra. The bands below 600 cm⁻¹ are attributed to the deformation vibrations of $\text{O}-\text{P}-\text{O}$ and can be probably

coupled to the corresponding asymmetric stretching modes of the cobalt oxygen bonds.^{25a}

UV-visible Absorption Spectroscopy. The UV-vis absorption spectrum of $\text{Co}_2\text{PO}_4\text{OH}$ (1) was recorded on a powder sample diluted by a 10-fold excess of BaSO_4 (Figure 3).

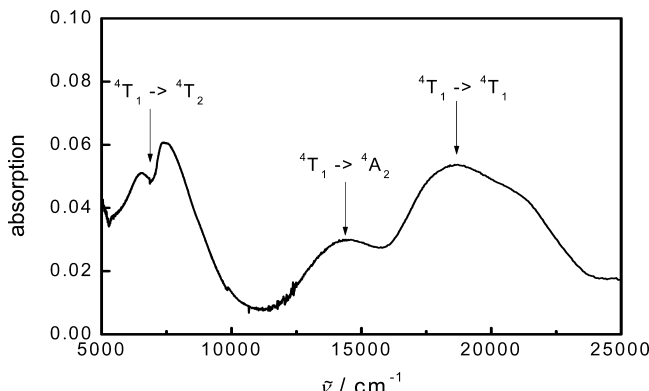


Figure 3. UV-vis absorption spectrum, measured in reflection on a powder sample of $\text{Co}_2\text{PO}_4\text{OH}$ (1) ground with a 10-fold excess of BaSO_4 . The arrows indicate the band positions used for further evaluation (see text).

As expected for $d^7 \text{Co}^{2+}$ in an octahedral-like coordination, three major transition bands are visible: the first one at 6860 cm^{-1} , which is split into two lines, the second one at $14\,390 \text{ cm}^{-1}$, and the third one at $18\,550 \text{ cm}^{-1}$ with a weak shoulder at $20\,900 \text{ cm}^{-1}$. This splitting can be explained by a Jahn-Teller distortion: reducing the symmetry from O_h to D_{4h} splits the T_{1g} levels into A_{2g} and E_g and the T_{2g} levels into B_{2g} and E_g .

Assuming purely octahedral environment, evaluation using Tanabe-Sugano diagrams for a d^7 system yields a Racah parameter of 850 cm^{-1} . This value is reduced to about 77% of the free ion value (1115 cm^{-1})²⁹ due to the nephelauxetic effect and is therefore well within the expected range. With this value a ligand-field splitting of 7800 cm^{-1} can be deduced.

Magnetism. Starting from the paramagnetic range observed around room temperature, the data is well-described by Curie-Weiss (CW) behavior (lower inset, Figure 4). From the CW fit a magnetic moment of $4.71 \mu_B$ per Co^{2+} ion is obtained, which is within expectations. For a spin-only $S = 3/2$ (d^7, Co^{2+}) a magnetic moment of $3.87 \mu_B$ is obtained, and for a Co^{2+} with full orbital contribution ($L + S = J$), the value can reach $5.2 \mu_B$. Hence, Co^{2+} in $\text{Co}_2\text{PO}_4\text{OH}$ has a significant orbital contribution (L) to the magnetic moment, but L is not fully evolved. The extracted Curie-Weiss constant ($\Theta_{\text{CW}} = -49.7 \text{ K}$) is negative, pointing to predominant antiferromagnetic interactions in the spin ground state. All of these observations agree with what has been measured for orthorhombic $\text{Co}_2\text{PO}_4\text{OH}$,³⁰ but the tetragonal modification exhibits other magnetic features at lower temperatures. As judged from both dc (Figure 4) and ac magnetic susceptibility data (upper inset Figure 4), the first magnetic anomaly starts to set in around 20 K . Note, the tetragonal modification is clearly different from the orthorhombic as the spin ordering at 71 K is missing here.³⁰ Below 20 K , the χ suddenly increases, indicating an emerging ferromagnetic spin component. Note that our tetragonal modification has a significantly larger molar susceptibility below 20 K compared to the orthorhombic one,³⁰ suggesting that a relatively strong spin canting is present in the antiferromagnetic state in tetragonal $\text{Co}_2\text{PO}_4\text{OH}$. The differ-

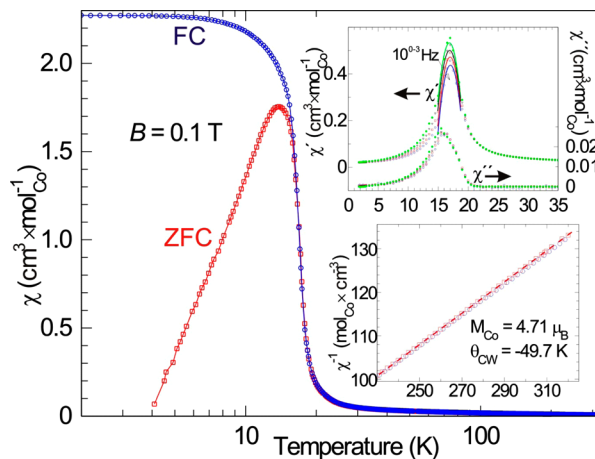


Figure 4. Magnetic susceptibility (χ) of tetragonal $\text{Co}_2(\text{PO}_4)(\text{OH})$ as function of temperature, displaying both field-cooled and zero-field-cooled data. The lower inset is a magnification of χ^{-1} at high temperatures including a Curie-Weiss fit (dashed line) together with the values obtained from that fit. Both real (χ') and imaginary (χ'') parts of χ are shown in the upper inset, where field driving frequency was increased from 1 to 1000 Hz, as indicated with a thin arrow close to the maximum in χ' .

ence between the field cooled (FC) and zero-field cooled (ZFC) data agrees well with a noticeable imaginary part of χ (upper inset, Figure 4) and indicates that magnetic domains are formed. The observed spin domains can be explained by examining the isothermal magnetizations performed at several different temperatures (Figure 5). At 30 K , the polarization at

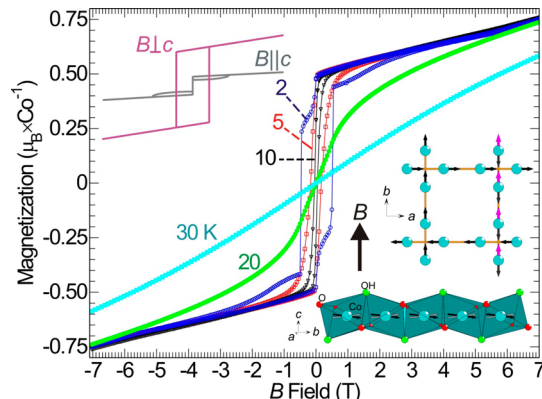


Figure 5. Magnetization as function of magnetic field (B) at several different temperatures, as indicated close to the corresponding curve. The upper-left curves represent the suggested magnetization anisotropy at 2 K , as discussed in the text for a theoretical single crystal. Both lower-right insets are structural motifs of tetragonal $\text{Co}_2\text{PO}_4\text{OH}$ with a suggested magnetic structure with black arrows and the magnetically induced states with B along c (gray arrows) and b (purple arrow).

highest field is no doubt weaker than at 20 K and below, which would suit a paramagnetic behavior, underlining the assumption that T_c is close to 20 K . As the temperature decreases from 20 to 5 K a remanent and a coercive field are observed, but the spin flips are smooth and progress in one step. The coercive field is larger than that in case of the dc and ac χ data, thus explaining the observed domain-like spin structure below T_c . In contrast, the magnetization data recorded at 2 K reveal a two-step process, although the size of the polarization at the highest

field does not change on going from 20 to 2 K. The absolute magnitude of the polarization is decisive for the spin ground state: a value of $0.75 \mu_B$ (Figure 5) of theoretically $3 \mu_B$ points to a ferri- or canted antiferro-magnetic ground state, which agrees with the fact that a negative θ_{CW} and a T_c (not a T_N) are observed. In tetragonal $\text{Co}_2\text{PO}_4\text{OH}$, for Co^{2+} there is only one crystallographically independent site (Wyckhoff symbol $8c$). Thus, assuming that no temperature-dependent structural transition is involved, the occurrence of a ferrimagnetic state is not likely as in that case an uneven contribution of magnetic moment of at least two crystallographically independent Co^{2+} sites is necessary. Thus, with only one crystallographic site present a canted antiferromagnetic spin order as the ground state is more likely.

The crystal structure of $\text{Co}_2\text{PO}_4\text{OH}$ features columns of tilted $[\text{CoO}_4(\text{OH})_2]$ octahedra face-shared by three oxygen atoms, running along the a ($= b$) axes (Figure 5). From the structure, two magnetic coupling paths can be identified: (i) the coupling along the columns and (ii) the coupling between the columns. The observed competing magnetic interactions thus can be explained if (i) is of a ferromagnetic and (ii) is of an antiferromagnetic nature (or vice versa). The magnetic structure of orthorhombic $\text{Co}_2\text{PO}_4\text{OH}$ contains ferromagnetic columns, as determined by neutron scattering.³⁰ Hence, all columns in the tetragonal modification are assumed to contain parallel coupled spins, and the 4_1 screw axis is conforming to a continuously rotating spin direction from one column to the next along the unique axis (inset, Figure 5).

Without further data, it is difficult to interpret the two steps in the 2 K magnetization data (Figure 5), especially from an isotropic powder. However, a complex spin-flip transition along a single crystallographic easy axis appears unlikely. Hence, it is fair to assume that the complex transition involves two components: one along the unique crystallographic axis (c) and a second perpendicular to it. Note that any in-plane ferromagnetic component has to break the tetragonal symmetry, and such a transition should be of first order, that is, hysteretic. Therefore it is possible to postulate that the hysteretic part of the transition belongs to a spin-flip in-plane ($\perp c$) component, and the nonhysteretic part is related to a spin-flop component oriented along the unique axis ($\parallel c$), shown in the lower-right inset in Figure 5. The size of the magnetization parts naturally corresponds to the relative amount of spins that are flipped or flopped, but more data are necessary to confirm these assumptions. However, by flipping one spin out of four within the ab plane, the magnetization changes by $0.75 \mu_B$ ($3 \mu_B/4$), which agrees quite well with the observations, considering that the measured sample is a powder with all crystallographic directions statistically equally represented. Neutron diffraction data would be necessary to fully understand the spin structure in tetragonal $\text{Co}_2(\text{PO}_4)\text{OH}$, and these investigations are planned in the near future.

CONCLUSIONS

A new framework cobalt phosphate, $\text{Co}_2\text{PO}_4\text{OH}$, has been successfully prepared under ionothermal conditions, using the IL 1-butyl-1-methylpyridinium hexafluorophosphate, $[\text{C}_4\text{mpy}]^-\text{[PF}_6^-]$, as the solvent and mineralizer. To allow for the determination of optical and magnetic behavior, phase-pure materials were obtained, and the optimal synthesis conditions were found by varying the stoichiometry of the reagents. $\text{Co}_2\text{PO}_4\text{OH}$ crystallizes in the tetragonal space group $I4_1/\text{amd}$.

It is built up by face-sharing Co octahedra chains parallel to the a and b axes, which are arranged in a simple cubic rod packing. The rods are linked through tribridging O(2)H atoms linking the Co octahedra to six-membered rings. Finally, PO_4 tetrahedra interconnect four chains of $\text{CoO}_4(\text{OH})_2$ octahedra. Further analytical methods such as FT-IR and UV-vis spectroscopy corroborate the crystal structure found. $\text{Co}_2\text{PO}_4\text{OH}$ stays thermally stable up to 400 °C in air. Magnetic susceptibility measurements show paramagnetic behavior near room temperature but an anomaly at about 20 K, which may be the compound's Curie temperature (T_c). A ferromagnetic moment arises below this temperature. Following the Curie-Weiss fit, considerations of crystallographic site occupancies of Co^{2+} , two magnetic coupling paths can be identified: one ferromagnetic along the columns and another antiferromagnetic between the columns. The spin ground state is probably canted antiferromagnetic. The magnetization curve observed at 2 K consists of a combination of a spin-flip and a spin-flop transition. Neutron diffraction measurements are necessary to unveil the magnetic structure-related details unambiguously.

ASSOCIATED CONTENT

S Supporting Information

Cif file, atomic parameter, X-ray diffraction pattern, TG curve, thermal ellipsoid plot, and atomic label schemes of compound 1. This material is available free of charge via the Internet at <http://pubs.acs.org>.

AUTHOR INFORMATION

Corresponding Author

*E-mail: anja.mudring@rub.de, mudring@iastate.edu. Phone: +49(0)234-32-27408. Fax: +49(0)234-32-14951.

Notes

The authors declare no competing financial interest.

ACKNOWLEDGMENTS

This Work is supported by the Deutsche Forschungsgemeinschaft (DFG) through SFB 608 and the Cluster of Excellence RESOLV. We thank Dr. P. S. Campbell for proof reading.

REFERENCES

- (1) Huminicki, D. M. C.; Hawthorne, F. C. *Rev. Mineral. Geochem.* **2002**, *48*, 123–253.
- (2) Pan, Y.; Fleet, M. E. *Rev. Mineral. Geochem.* **2002**, *48*, 13–50.
- (3) (a) Lii, K.-H.; Huang, Y.-F.; Zima, V.; Huang, C.-Y.; Lin, H.-M.; Jiang, Y.-C.; Ling, F.; Wang, L. *Chem. Mater.* **1998**, *10*, 2599–2609. (b) Fur, E. Le; Riou, A.; Pena, O.; Pivan, J. Y. *Solid State Sci.* **2000**, *2*, 135–141.
- (4) Bhaumik, A.; Inagaki, S. *J. Am. Chem. Soc.* **2001**, *123*, 691–696.
- (5) Yu, D. H.; Wu, C.; Kong, Y.; Xue, N. H.; Guo, X. F.; Ding, W. P. *J. Phys. Chem. C* **2007**, *111*, 14394–14399.
- (6) Maspoch, D.; Ruiz-Molina, D.; Veciana, J. *Acc. Chem. Res.* **2007**, *36*, 770–818, and references therein.
- (7) Stucky, G. D.; Phillips, M. L. F.; Gier, T. E. *Chem. Mater.* **1989**, *1*, 492–509.
- (8) Masquelier, C.; Croguennec, L. *Chem. Rev.* **2013**, *113*, 6552–6591.
- (9) Hogarth, C. A.; Basha, M. J. *J. Phys. D: Appl. Phys.* **1983**, *16*, 869–878.
- (10) (a) Lee, W. H.; Seo, Y.; Bishop, P. L. *Sens. Actuators, B* **2009**, *137*, 121–128. (b) Kanan, M. W.; Surendranath, Y.; Nocera, D. G. *Chem. Soc. Rev.* **2009**, *38*, 109–114. (c) Dimesso, L.; Foerster, C.; Jaegermann, W.; Khanderi, J. P.; Tempel, H.; Popp, A.; Engstler, J.;

Schneider, J. J.; Sarapulova, A.; Mikhailova, D.; et al. *Chem. Soc. Rev.* **2012**, *41*, 5068–5080.

(11) (a) Feng, P.; Bu, X.; Stucky, G. D. *Nature* **1997**, *388*, 735. (b) Bu, X.; Feng, P.; Stucky, G. D. *Science* **1997**, *278*, 2080–2085.

(12) (a) Choudhury, A.; Neeraj, S.; Natarajan, S.; Rao, C. N. R. *Angew. Chem., Int. Ed.* **2000**, *39*, 3091–3093. (b) Chiang, R.-K. *Inorg. Chem.* **2000**, *39*, 4985–4988. (c) Chang, W. K.; Chiang, R. K.; Jiang, Y. C.; Wang, S. L.; Lee, S. F.; Lii, K. H. *Inorg. Chem.* **2004**, *43*, 2564–2568. (d) Karmakar, D.; Yakhmi, J. V. *J. Phys.: Condens. Matter* **2012**, *24*, 436003/1–436003/9.

(13) (a) Chen, J. S.; Jones, R. H.; Natarajan, S.; Hursthouse, M. B.; Thomas, J. M. *Angew. Chem., Int. Ed.* **1994**, *33*, 639–640. (b) Natarajan, S.; Neeraj, S.; Choudhury, A.; Rao, C. N. R. *Inorg. Chem.* **2000**, *39*, 1426–1433. (c) Yuan, H. M.; Chen, J. S.; Zhu, G. S.; Li, J. Y.; Yu, J. H.; Yang, G. D.; Xu, R. R. *Inorg. Chem.* **2000**, *39*, 1476–1479. (d) Natarajan, S.; Neeraj, S.; Rao, C. N. R. *Solid State Sci.* **2000**, *2*, 87–89.

(14) (a) Lorbeer, C.; Mudring, A.-V. *J. Phys. Chem. C* **2013**, *117*, 12229–12238. (b) Campbell, P. S.; Lorbeer, C.; Cybinska, J.; Mudring, A.-V. *Adv. Funct. Mater.* **2013**, *23*, 2924–2931. (c) Alammar, T.; Shekhah, O.; Mudring, A.-V. *J. Mater. Chem.* **2012**, *22*, 18252–18260. (d) Richter, K.; Birkner, A.; Mudring, A.-V. *Angew. Chem., Int. Ed.* **2010**, *49*, 2431–2435.

(15) Mudring, A. V.; Wang, G. *Abstracts of Papers*, 243rd National Meeting and Exposition of the American Chemical Society, San Diego, CA, United States, March 25–29, 2012; American Chemical Society: Washington, DC, 2012.

(16) Wang, G.; Mudring, A.-V. *Crystals* **2012**, *1*, 22–27.

(17) Wang, G.; Valldor, M.; Lorbeer, C.; Mudring, A.-V. *Eur. J. Inorg. Chem.* **2012**, *18*, 3032–3038.

(18) X-Red 1.22, Stoe Data Reduction Program (C); Stoe & Cie GmbH: Darmstadt, Germany, 2001.

(19) X-Shape 1.06, Crystal Optimization for Numerical Absorption Correction (C); Stoe & Cie GmbH: Darmstadt, Germany, 1999.

(20) (a) Sheldrick, W. S. *SHELXTL Program*, version 5.1; Siemens Industrial Automation, Inc.: Madison, WI, 1997. (b) Sheldrick, G. M. *Acta Crystallogr.* **2008**, *A64*, 112–122.

(21) Keefer, K. D.; Hochella, M. F., Jr.; DeJong, B. H. W. S. *Acta Crystallogr.* **1981**, *B37*, 1003–1006.

(22) Leblanc, M.; Collin-Fèvre; Férey, G. *J. Magn. Magn. Mater.* **1997**, *167*, 71–79.

(23) Waldrop, L. *Naturwissenschaften* **1968**, *55*, 178.

(24) O'Keefe, M.; Andersson, S. *Acta Crystallogr.* **1977**, *A33*, 914–923.

(25) (a) Pedro, I. de; Rojo, J. M.; Lezama, L.; Rojo, T. Z. *Anorg. Allg. Chem.* **2007**, *633*, 1847–1852. (b) Pedro, I. de; Rojo, J. M.; Fernández, J. R.; Lezama, L.; Rojo, T. *Eur. J. Inorg. Chem.* **2010**, 2514–2522.

(26) (a) Hill, R. M.; Ichiki, S. K. *J. Chem. Phys.* **1968**, *48*, 838–842. (b) Hammer, V. M. F.; Libowitzky, E.; Rossman, G. R. *Am. Mineral.* **1998**, *83*, 569–576.

(27) Nakamoto, K. In *Infrared and Raman Spectroscopy of Inorganic and Coordination Compounds Part B*, 6th ed.; John Wiley & Sons: New York, 2009, P62.

(28) Bontchev, R. P.; Iliev, M. N.; Dezaneti, L. M.; Jacobson, A. J. *Solid State Sci.* **2001**, *3*, 133–142.

(29) McClure, D. S. *Solid State Phys.* **1959**, *9*, 399–525.

(30) Rojoetal Rojo, J. M.; Mesa, J. L.; Lezama, L.; Pizarro, J. L.; Arriortua, M. I.; Rodriguez Fernandez, J.; Barberis, G. E.; Rojo, T. *Phys. Rev. B: Condens. Matter Mater. Phys.* **2002**, *66*, 094406/1–094406/13.